Dilatancy in Slow Granular Flows

Alexandre J. Kabla*
Department of Engineering, University of Cambridge, Trumpington Street, Cambridge CB2 1PZ, UK

Tim J. Senden
Department of Applied Mathematics, Research School of Physical Sciences and Engineering, The Australian National University, Canberra, 0200 Australia
(Dated: October 8, 2008)

When walking on wet sand, each footstep leaves behind a temporarily dry impression. This counter intuitive observation is the most common illustration of the Reynolds principle of dilatancy: that is, a granular packing tends to expand as it is deformed. As a consequence, the amount of porous space increases, resulting in the apparent drying of the footprint. Although widely called upon in areas such as soil mechanics, geomechanics, as well as many industrial processes, a deeper understanding of this principle is constrained by the lack of analytical techniques to study this behaviour. Using X-ray radiography we track a broad variety of granular flow profiles and quantify their intrinsic dilatancy behaviour. These measurements frame Reynolds dilatancy as a kinematic process. Closer inspection demonstrates however the practical importance of flow induced compaction which competes with dilatancy, leading more complex flow properties than expected.

PACS numbers: 83.80.Fg 83.50.-v 83.60.-a

The impact of granular flows on our daily lives is often understated, yet they represent the second most common material displaced by humans. Consideration of just a few of these activities such as the efficient transport of grain, the optimal compaction of building materials and the prediction of rock slides demonstrates the strikingly complex behaviour of these materials. Many of these global phenomena have been studied in detail, to mention a few; finite angle of repose and avalanching [1], spontaneous jamming [2], dilatancy [3], compaction [4], shear banding [5] or grain segregation [6]. However, theoretical advances are hampered by fundamental problems such as history dependant effects or heterogeneous flow profiles, stressing the need for new tools to define and measure intrinsic local parameters.

The phenomenon of dilatancy [3] corresponds to the decrease of a grain pile's density upon shear. The intuitive interpretation is that free volume is required for grains to rearrange. This property is typically quantified at small deformation by simple shearing a sample and measuring the ratio between imposed boundary displacement and resulting thickness change at constant pressure [7]. However, efficient flow predictions rely on the determination and testing of constitutive equations valid up to large deformations, where flow profiles need to be characterized. Along that line, dilatancy during shear band formation has been recently highlighted [8, 9], but a general framework for dilatancy in granular flows is still needed. An outstanding issue, for instance, is to determine to which extent dilatancy is a material property, quantitatively independent on the flow conditions. At present theories are insufficient to aid such practical predictions and we must turn to experiment to guide us.

We introduce here an experimental approach which combines real time X-ray radiography and DIC (Digital Image Correlation) techniques to locally quantify both density variations and strain tensors in a range of 3D granular flows. In particular, we have studied gravity flows and forced shear flows. Flows are generated in rectangular containers, typically 5cm wide, 3cm thick, 20cm high and filled with millimetric grains. In the forced shear experiment, we use a particular geometry where a rigid bracket moves slowly upward while a small wall prevents grains from falling below the bracket (Fig. 1a). The bracket and the opposite wall are fully covered by bound grains to maximize friction. As discussed later, the complexity of the resulting flow profile is a key element to probe the generality of our observations. The gravity driven experiment consists of a large smooth wall moving upward in a similarly dimensioned container as before (Fig. 1b). Withdrawing the partition progressively frees space below it such that grains are free to flow into the void. Unlike the first configuration, the grains freely slip against the walls. In both situations, flows are invariant along the cell thickness and studied in the quasistatic limit, the walls being moved incrementally at speeds of about 0.1mm s^{-1}.

X-Ray absorption has been broadly used to quantify minute density variations in 3D piles, for instance to study compaction [10] or the onset of shear-banding [11]. Recent progress in real time X-ray imaging also allowed to study more dynamic processes such as pre-avalanche dynamics [12]. We use here the same setup as in [12] (Fig. 1c) to take radiographic series of the cells while the flow is in progress. The intensity in a typical radiograph takes the following form:

$$I(x,y,t) = I_0(x,y,t) \cdot \exp\left(-\frac{L_g(x,y,t)}{\lambda_g}\right) \qquad (1)$$

*Electronic address: ajk61@cam.ac.uk

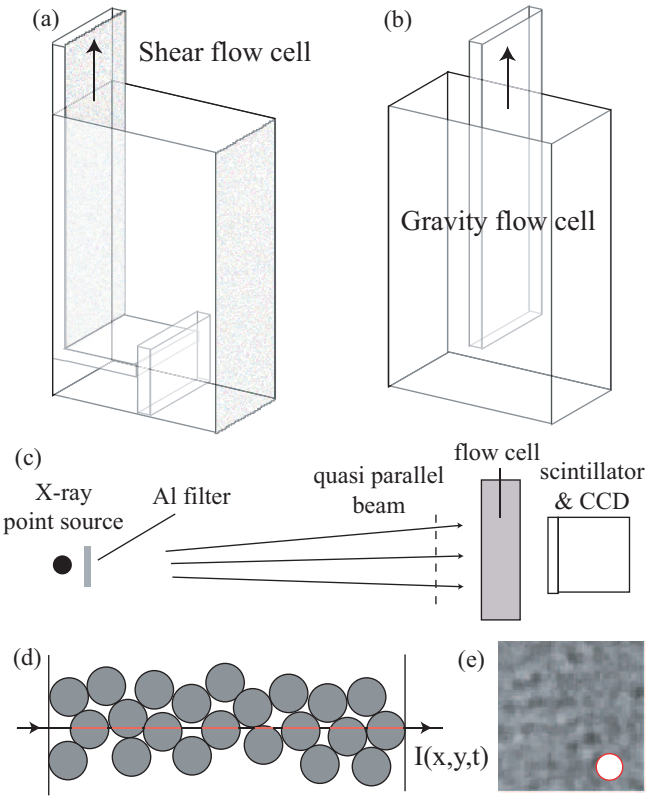

FIG. 1: (a) Shear flow cell. (b) Gravity flow cell. (c) X-ray images acquisition setup. Source settings: 80kV and 150μA. A 2mm Al filter reduces beam hardening. The cell is 2.3m away from the source, ensuring a quasi-parallel beam. (d) Illustration of the path of an X-ray and (e) resulting material length image $L_g(x, y)$. Circle indicates the grain size.

where $L_g(x, y, t)$ represents the local length of grain crossed by the X-ray beam at the coordinates (x, y) (Fig. 1d), λ_g corresponds to the absorption coefficient of the grain material (assuming the absorption is uniform in the beam spectrum); it is measured independently. $I_0(x, y, t)$ accounts for the angular variation in X-ray source intensity, the source temporal intensity fluctuations, as well as the absorption of the container itself and variations in detector sensitivity across the face of the detector. To determine $I_0(x, y, t)$, we record radiographs $I_{wg}(x, y, t)$ with an empty container in exactly the same geometrical configuration. $I_0(x, y, t)$ and $I_{wg}(x, y, t)$ are identical images, only scaled by the random intensity fluctuations of the source: $I_{wg}(x, y, t) = \alpha(t)I_0(x, y, t)$. We use a region S of the image where grains are absent, i.e. where $I(x, y, t) = I_0(x, y, t)$, to quantify the source fluctuation $\alpha(t) = \langle I_{wg}(x, y, t)/I(x, y, t)\rangle_S$. The local grain thickness is then provided by:

$$L_g(x, y, t) = \lambda_g \cdot \ln\left(\frac{I_{wg}(x, y, t)}{\alpha(t)I(x, y, t)}\right) \qquad (2)$$

The average grain density over an arbitrary domain D which spans the sample thickness is directly obtained from $\langle\rho(x, y, t)\rangle_D = \langle L_g(x, y, t)\rangle_D / L$ where L is the gap between the front and rear walls of the container.

We use DIC to determine the displacement field $\vec{u}(\vec{x}, t)$ between two images and reconstruct material point trajectories during whole experiments. This method is increasingly used to quantify strain fields in complex or composite media such as fibre structures [13], biological tissues [14] and granular materials [8]. In our case, the grain thickness L_g and density images exhibit a noise pattern at the grain scale (Fig. 1e), with a contrast of the order of R/L, where R is the grain size. This spatial pattern is a signature of the local 3D structure of the packing and is advected with the grains, although it progressively evolves with the strain. In practice, displacement increments around half a grain diameter and total pile thickness of up to 50 grains provide robust measurement conditions for correlation methods.

Using the flow trajectories, we determine the evolution of local domains arranged on a grid, and quantify for each of them, at each instant, the local density and total strain taking the initial state as a reference. Figure 2 shows the typical flow and density profiles for both flow cells. The initial configuration was prepared by slowly pouring grains into the container while mechanically tapping the cell. This protocol provides initial packing fractions about 0.64 with a suitable homogeneity across the cell. Both experiments exhibit strong correlations between the local deformation and the packing fraction variation. The local shear is accounted for by the deviatoric component of the 2D strain tensor; the volumetric component is redundant with, and less precise than, the density measurement. The shear, quantified by a scalar s, is calculated from the eigenvalues λ_1 and λ_2 of the logarithmic strain tensor for finite deformations [15]: $s = |\lambda_1 - \lambda_2|/2$. Figure 3 shows in a scatter plot the local values of the packing fraction and shear s, for all domains, all times, for the two flow cells, and for two grain sizes. The two configurations allow a broad range of different shear histories and stress states. This scatter plot defines a master curve relating the local strain and density change up to large deformations. The data can be conveniently fitted by an empirical exponential relationship that defines the critical deformation s_c after which the steady state regime is locally reached:

$$\rho(\epsilon) = \rho_{min} + (\rho_{max} - \rho_{min}) \exp(-s/s_c) \qquad (3)$$

The pile response remains qualitatively unchanged with different grain shapes and/or larger polydispersity (Fig. 4a and 4b), the value of critical deformation s_c being systematically about 0.2-0.3. These results indicate that Reynolds dilatancy can be summarized by a local kinematic relationship, supporting a number of theoretical and numerical approaches [16, 17]. Our setup provides a generic and robust way to extract the empirical parameters such as limiting densities and critical strains. In contrast with traditional shearbox tests where the shear zone is undetermined [7], the characterisation

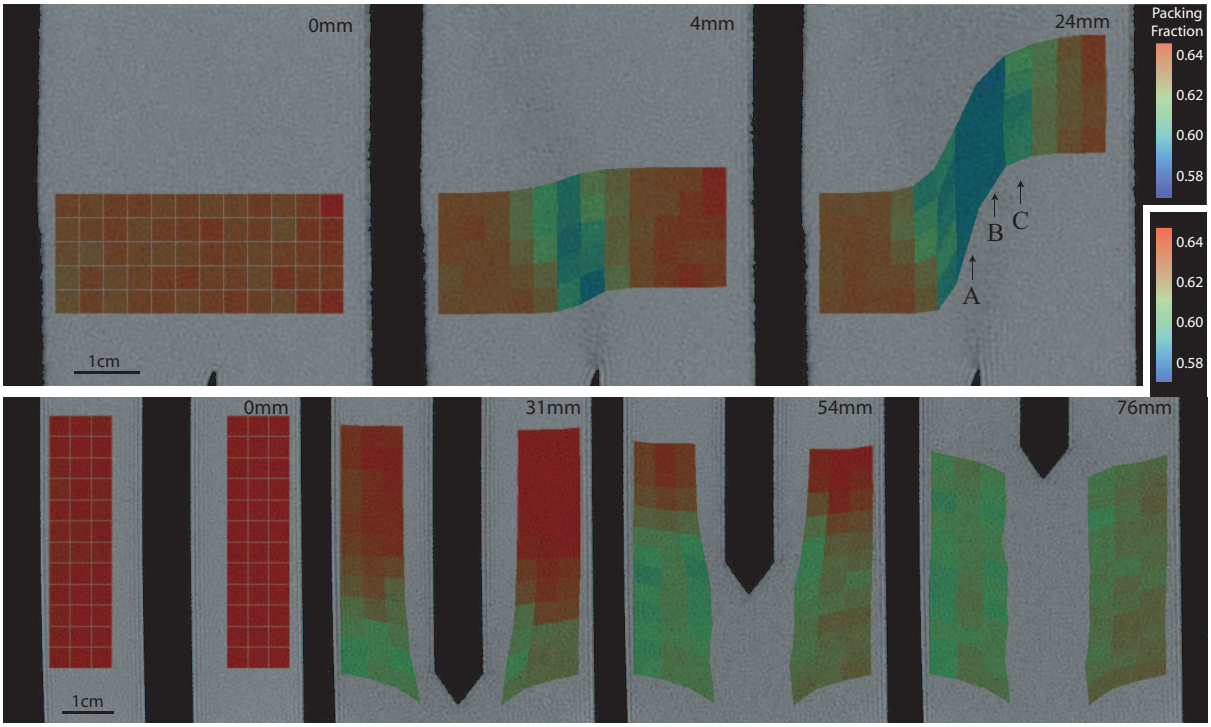

FIG. 2: Series of radiographs describing the flow and density profiles for a shear flow (top) and gravity driven flow (bottom). Material: monodisperse acrylic spheres, 1mm in diameter. Numbers on the top right corner of each image indicate the upward displacement of the moving wall. See EPAPS Movies No. 1 and 2 for the complete sequence of images. Letters designate specific regions discussed in the text and Fig. 4b.

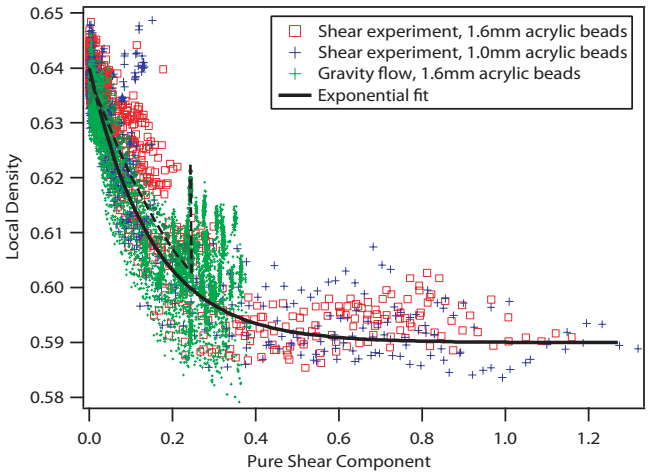

FIG. 3: Evolution of the local density as a function of the local shear for various geometries and bead sizes; Piles have been compacted before the experiment starts. The scale for the density (i.e. the value of the absorption length) is measured with $\pm 0.5\%$ accuracy. The black dashed line guides the eye along one specific domain trajectory for the gravity flows.

here takes into account the heterogeneity of the flow profile and produces well defined material properties.

If the same experiments are repeated with loose sphere piles (see Fig. 4c), the material compacts as expected at small strains [18]. However, it rapidly reaches a steady density similar to that previously reported, the values being scattered mostly between 0.59 and 0.6. The critical state picture [7], which posits the existence of a particular packing fraction at which shear can be sustained without change in volume being independent of either the initial state or deformation mode, is confirmed here by our experiments.

Although true on a local scale this conclusion requires qualification. In the gravity flow experiment, nearly all the regions experience a significant increase of the density following the shear-induced expansion (see dashed line in Fig. 3). This process is known as compaction and corresponds to the intrinsic response of a granular pile to mechanical taps or vibrations [4, 19]. Such fluctuations arise in our experiments in the vicinity of flowing regions and cause frequent reorganisation of the force network. A similar yet more subtle effect is observed in the forced shear experiments. The packing fraction for a given shear value slightly increases with the distance to the shear band (see dashed lines in Fig. 4b); this again contradicts the existence of a well defined relationship between shear strain and density. Although different regions experience different shear rates, this cannot account for the difference in behaviour in a quasistatic experiment. The caution comes in considering the competition of local compaction and dilatancy during shear. The gravity driven experiment, for example, shows that the flow in the shear

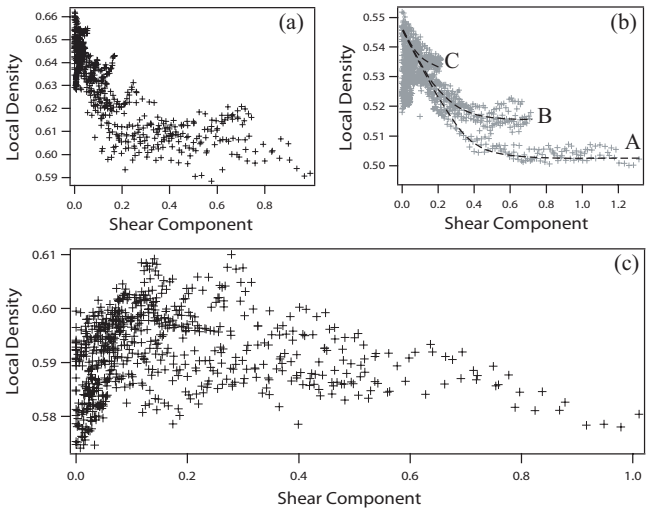

FIG. 4: Evolution of the local density as a function of the local shear for various materials and initial densities. (a) Shear experiment with monodisperse pasta cylinders, 2mm long, 2mm in diameter. (b) Shear experiment with polydisperse semolina grains, diameters ranging from 0.5 to 1 mm. The dashed lines represent the typical behaviours of the regions A, B and C defined on Fig. 2. Due to the nature of these materials, errors on the absolute value of the densities may be up to 10%, however relative variations are precise up to 0.1% (c) Shear experiment with 1mm acrylic monodisperse beads, starting with a low density pile.

band can generate stress fluctuations able to cause compaction in remote regions. In the shear band, compaction effects are negligible because it deforms over a time scale where the rest of the sample is mostly static. Away from the shear band we observe a range of situations where material is being sheared and simultaneously mechanically shaken by the stress fluctuations coming from the shear band. The effect is, as observed, an increase of the resulting density for a given shear strain. In regions where dilatancy competes with compaction, the critical state may never be reached, even after large shear.

The experimental configuration detailed here offers numerous improvements to the quantification of the flow/density relationships in granular matter. We demonstrate that, to a first approximation, dilatancy of dense pile can be considered as a kinematic property, with different flow situations providing consistent behaviour. This can be applied to a wide range of materials and geometries, up to very large deformations, although the study of non-isotropic grains would require a more complex framework. Interestingly, these experiments also unveil the intricate interplay between Reynold's dilatancy and compaction in complex granular flows. The dilatancy curve measured in shear bands only defines a lower bound to the range of available densities. To characterize the response of the material in other regions, one needs to understand how mechanical fluctuations are generated, propagate and cause compaction. Although nonlocal elastic fluctuations have been derived from the flow profile in systems like foams [20], such a question represents a major challenge in the context of granular flows where the mechanisms of force propagation and microplasticity are still poorly understood. Nevertheless, this appears to be a key to predict both the density profile and stability of granular flows.

Acknowledgments

The authors would like to thank Tomaso Aste, Georges Debrégeas and L. Mahadevan for discussions. TJS gratefully acknowledges the Australian Research Council for support.

[1] H.M. Jaeger, C.H. Liu and S.R. Nagel, Phys. Rev. Lett., **62**, 40 (1989).
[2] K. To, P-Y Lai and H.K. Pak, Phys. Rev. Lett., **86**, 71 (2001).
[3] O. Reynolds, Phil. Mag. **20**,469 (1885).
[4] J. B. Knight, C. G. Fandrich, C. N. Lau, H. M. Jaeger and S. R. Nagel, Phys. Rev. E **51**, 3957 (1995).
[5] J. Desrues and R. Chambon, Int. J. of Sol. and Struct., **39**, 3757 (2002).
[6] Y. Oyama, Bull. Inst. Phys. Chem. Res. Jpn. Rep. **18**, 600 (1939).
[7] W. Powrie, Soil Mechanics: concepts and applications,second edition, Spon Press, London (2004).
[8] Rechenmacher, J. Mech. Phys. Solids **54**, 22 (2006).
[9] K. Sakaie, D. Fenistein, T. J. Carroll, M. van Hecke and P. Umbanhowar, arXiv.org:0704.3745.
[10] P. Philippe and D. Bideau, Europhys. Lett. **60**, 677 (2002).
[11] J. Desrues, R. Chambon, M. Mokni and F. Mazerolle, Geotechnique **46**, 529 (1996).
[12] A. Kabla, G. Debrégeas, J.M. di Meglio and T.J. Senden, Europhys. Lett. **71**, 932 (2005)
[13] S. Bergonnier, F. Hild and S. Roux, J. of Strain Analysis for Eng. Design. **40**, 185 (2005).
[14] C. Wiebe and G.W. Brodland, J. of Biomech. **38**, 2087 (2005).
[15] S. Nemat-Nasser, Plasticity, Cambridge University Press (2004).
[16] J.D. Goddard and A.K. Didwania, Q. J. Mech. Appl. Math. **51**, 15 (1998).
[17] I.F. Collins and B. Muhunthan, Géotechnique **53**, 611 (2003).
[18] M. Nicolas, P. Duru and O. Pouliquen, Eur. Phys. J. E **3**, 309 (2000).
[19] A. Kabla and G. Debrégeas, Phys. Rev. Lett. **92**, 035501 (2004).
[20] A. Kabla, J. Scheibert and G. Debrégeas, J. Fluid. Mech. **587**, 45 (2007).